Leucine-rich repeat containing 8A (LRRC8A) is essential for T lymphocyte development and function

Lalit Kumar,[1,3] Janet Chou,[1,3] Christina S.K. Yee,[1,3] Arturo Borzutzky,[1,3] Elisabeth H. Vollmann,[4] Ulrich H. von Andrian,[4] Shin-Young Park,[2,5] Georg Hollander,[6,7] John P. Manis,[2,5] P. Luigi Poliani,[8] and Raif S. Geha[1,3]

[1]Division of Immunology and [2]Joint Program in Transfusion Medicine, Division of Laboratory Medicine, Boston Children's Hospital; and [3]Department of Pediatrics, [4]Department of Microbiology and Immunobiology, and [5]Department of Pathology, Harvard Medical School, Boston, MA 02115
[6]Department of Pediatrics and the [7]Weatherall Institute of Molecular Medicine, Oxford OX3 9DU, England, UK
[8]Department of Molecular and Translational Medicine, Pathology Unit, University of Brescia, 25124 Brescia, Italy

Lrrc8a **is a ubiquitously expressed gene that encodes a leucine-rich repeat (LRR)–containing protein detected at higher levels on the surface of thymocytes than on other immune cells. We generated** ***Lrrc8a*****$^{-/-}$ mice to investigate the role of LRRC8A in lymphocyte development and function.** ***Lrrc8a*****$^{-/-}$ mice had increased prenatal and postnatal mortality, growth retardation, and multiple tissue abnormalities.** ***Lrrc8a*****$^{-/-}$ mice displayed a modest block in B cell development but intact intrinsic B cell function. In contrast, both** ***Lrrc8a*****$^{-/-}$ mice and** ***Lrrc8a*****$^{-/-}$$\rightarrow$*****Rag2*****$^{-/-}$ bone marrow chimeras exhibited a severe cell-intrinsic block in early thymic development, with decreased proliferation and increased apoptosis of thymocytes, and impaired peripheral T cell function. Thymic epithelial cells expressed an LRRC8A ligand that was critical for double-negative to double-positive thymocyte differentiation and survival in vitro. LRRC8A constitutively associated with the GRB2–GAB2 complex and lymphocyte-specific protein tyrosine kinase (LCK) in thymocytes. LRRC8A ligation activated AKT via the LCK–ZAP-70–GAB2–PI3K pathway, and AKT phosphorylation was markedly reduced in the thymus of** ***Lrrc8a*****$^{-/-}$ mice. These findings reveal an essential role for LRRC8A in T cell development, survival, and function.**

CORRESPONDENCE
Raif S. Geha:
raif.geha@childrens.harvard.edu

Abbreviations used: AIRE, autoimmune regulator; cTEC, cortical TEC; DN, double negative; DP, double positive; GST, glutathione S-transferase; LCK, lymphocyte-specific protein tyrosine kinase; LRR, leucine-rich repeat; mTEC, medullary TEC; SP, single positive; TEC, thymic epithelial cell; TUNEL, TdT-mediated dUTP nick end labeling; UEA-1, ulex europeus agglutinin 1.

Leucine-rich repeats (LRRs) are 20–29-aa-long sequences that contain a conserved consensus sequence LxxLxLxxN/CxL, where L may be replaced by isoleucine, phenylalanine, or valine (Kobe and Kajava, 2001). LRRs provide a structural framework for protein–protein interactions (Kobe and Kajava, 2001). Several LRR-containing proteins, such as TLRs, NODs, and GP1bβ, are important in innate immunity (Tang et al., 2004; Inohara et al., 2005; Lee and Kim, 2007). Little is known about the role of LRR-containing proteins in adaptive immunity, with the exception of CIITA (MHC class II transactivator), the deficiency of which results in absent expression of MHC class II molecules and severe immunodeficiency (Cressman et al., 1999).

LRRC8A (LRR containing 8A) is a 94-kD LRR-containing protein highly conserved between human and mouse (Sawada et al., 2003). LRRC8A spans the cell membrane four times and its extracellular C terminus contains 17 LRRs (Sawada et al., 2003; Smits and Kajava, 2004). A 17-yr-old female patient with congenital facial abnormalities, absent B cells, and agammaglobulinemia, but normal numbers of T cells, had a balanced t(9;20)(q33.2;q12) translocation, resulting in the deletion of the C-terminal two-and-a-half LRRs of LRRC8A (91 aa) and the addition of 35 aa derived from an intronic sequence (Sawada et al., 2003). The truncated *LRRC8A* product was co-expressed with the intact product of the normal *LRRC8A* allele at comparable levels (Sawada et al., 2003). Reconstitution of irradiated recipient mice with

The Rockefeller University Press $30.00
J. Exp. Med. 2014 Vol. 211 No. 5 929-942
www.jem.org/cgi/doi/10.1084/jem.20131379

The Journal of Experimental Medicine

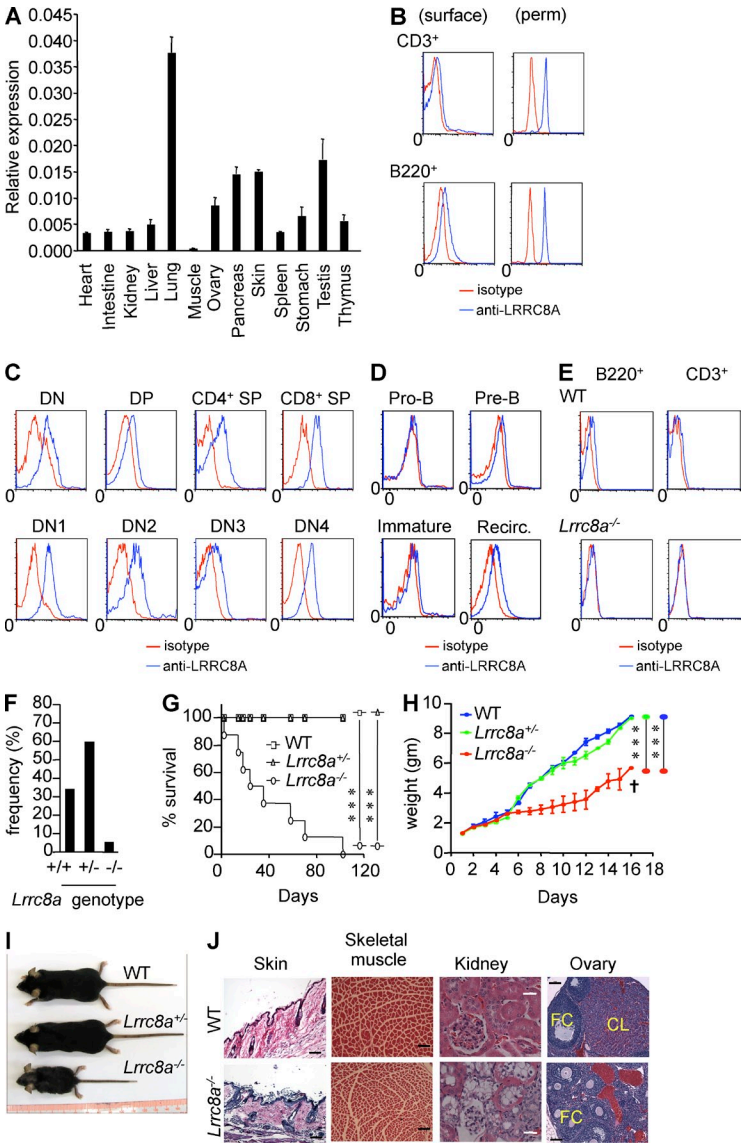

Figure 1. Expression of LRRC8A in C57BL/6 mice and survival, morphology, and tissue histology of *Lrrc8a*$^{-/-}$ mice. (A) Q-PCR analysis of *Lrrc8a* mRNA expression in tissues. *Lrrc8a* mRNA levels are expressed relative to *Gapdh* mRNA levels. (B) FACS analysis of LRRC8A surface and intracellular expression on electronically gated splenic CD3$^+$ cells B220$^+$ cells using polyclonal antibody C18. Perm: permeabilized. (C and D) FACS analysis of LRRC8A surface expression by subpopulations of thymocytes (C) and BM B cells (D) using polyclonal antibody C18. (E) FACS analysis of LRRC8A expression on gated splenic CD3$^+$ cells B220$^+$ cells from *Lrrc8a*$^{-/-}$ mice and WT littermates. (F) Frequency of WT, *Lrrc8a*$^{+/-}$, and *Lrrc8a*$^{-/-}$ pups obtained from the matings of *Lrrc8a*$^{+/-}$ mice (n = 622 pups). (G) Kaplan-Meier analysis of survival of 120 F_2 offspring born from matings of *Lrrc8a*$^{+/-}$ mice, which included 8 *Lrrc8a*$^{-/-}$, 72 *Lrrc8a*$^{+/-}$, and 40 *Lrrc8a*$^{+/+}$ littermates. (H) Body weight of *Lrrc8a*$^{-/-}$ mice and of *Lrrc8a*$^{-/+}$ and WT littermates (6 mice per group). (I) Gross appearance of WT, *Lrrc8a*$^{+/-}$, and *Lrrc8a*$^{-/-}$ mice at 5 wk of age. (J) Representative H&E-stained tissue sections from skin, skeletal muscle, and ovary (bars, 200 µm), and kidney (bars, 100 µm) of *Lrrc8a*$^{-/-}$ mice and WT littermates. FC: follicle, CL: corpus luteum. Data are representative of three independent experiments with one mouse per group (A, C, and D), six independent experiments with one mouse per group (B and E), two independent experiments with 3 mice per group (H and I), and two independent experiments with two mice per group (J). Mean and SEM are shown in A and H. ***, P < 0.001 (Student's t test).

syngeneic CD34$^+$ BM progenitors transduced with a retroviral vector overexpressing the mutant *LRRC8A* resulted in a severe block in B cell development at the pro–B cell to pre–B cell transition and reduced numbers of T cells (Sawada et al., 2003). The phenotype was attributed to the dominant negative effect of the co-expressed mutant *LRRC8A* allele (Conley, 2003; Sawada et al., 2003). No developmental or functional analysis of the T cells was conducted in these mice, and the expression level of the mutant protein in hematopoietic cells was not documented (Sawada et al., 2003).

To understand the role of LRRC8A in the adaptive immune system, we generated *Lrrc8a*$^{-/-}$ mice that expressed no LRRC8A protein. Unlike the patient, *Lrrc8a*$^{-/-}$ mice have peripheral B cells and normal immunoglobulin levels but display a severe cell-intrinsic block in thymic development and impaired peripheral T cell function. We demonstrate that thymic epithelial cell (TECs) express ligands for LRRC8A and that LRRC8A ligation activates AKT via the lymphocyte-specific protein tyrosine kinase (LCK)–ZAP-70–GAB2–PI3K pathway. Our work demonstrates an essential role for LRRC8A in T cell development and function.

RESULTS

Lrrc8a is widely expressed and LRRC8A is highly expressed on thymocytes compared with other immune cells

Lrrc8a mRNA was detected in all 13 tissues tested (Fig. 1 A). We examined cellular expression of LRRC8A using a rabbit polyclonal antibody to the C-terminal 18-aa-long peptide of LRRC8A, and a mAb, 4D10, directed against the region between the second and third putative transmembrane domains (aa 147–262) of LRRC8A. FACS analysis using these two antibodies readily detected LRRC8A on the surface of 293T cells transfected with a vector encoding LRRC8a, but not empty vector (Fig. S1 A), indicating that LRRC8A can be expressed on the cell surface, and that both the N and C termini

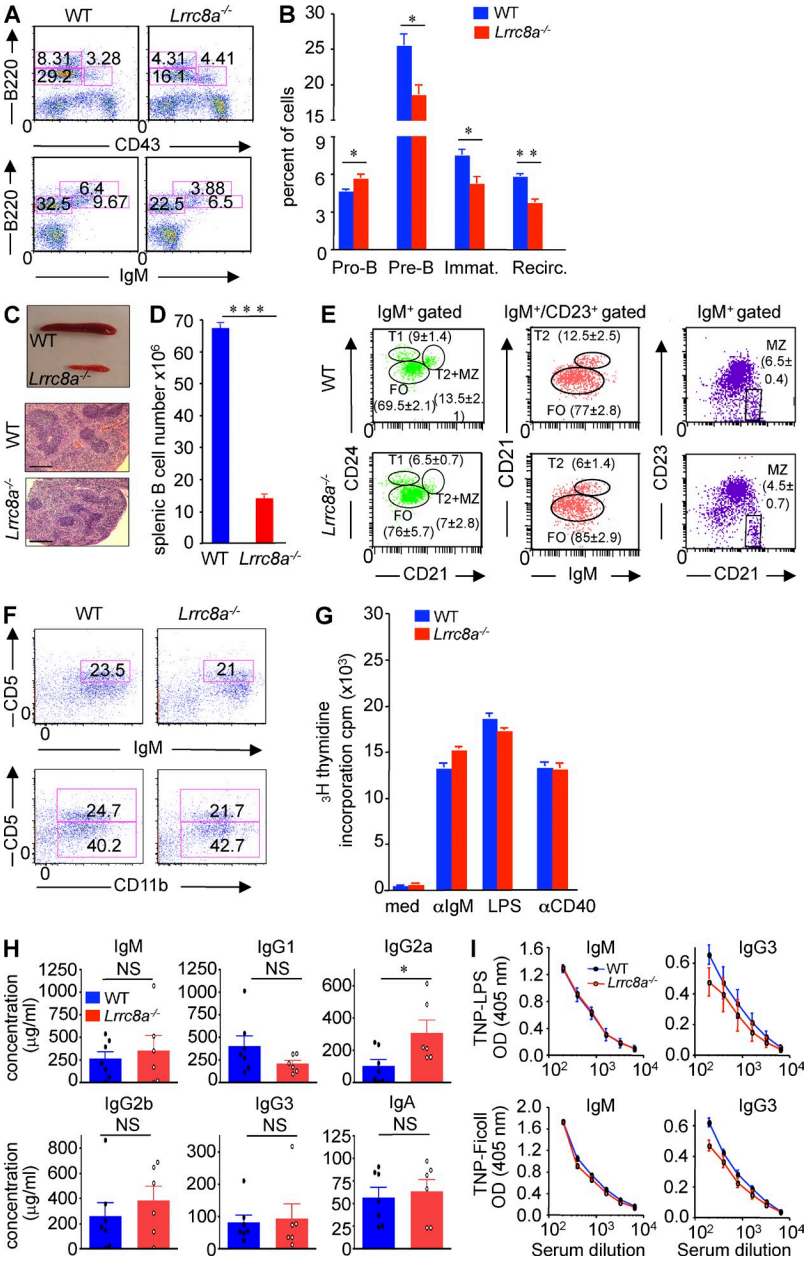

Figure 2. B cell development and function in *Lrrc8a*$^{-/-}$ mice. (A and B) FACS analysis (A) and percentage (B) of B cell subpopulation in the BM (Immat.: immature, Recirc.: recirculating). (C–E) Gross appearance and H&E staining (bars, 200 µm; C), numbers of B220$^+$ cells in spleens (D), and FACS analysis of CD21 and CD24 expression by sIgM$^+$ cells (E, left), of sIgM and CD21 expression by sIgM$^+$CD23$^+$ cells (E, middle), and of CD21 and CD23 expression by sIgM$^+$ cells (E, right). (F) FACS analysis of peritoneal lavage fluid for IgM$^+$CD5$^+$ B1 cells (top) and for CD5 and CD11b (bottom), within the gated B220$^+$ cell population. (G) ^{3}H-thymidine incorporation in purified splenic B cells after anti-IgM, LPS, and anti-CD40 stimulation for 72 h. med.: medium. (H) Serum levels of immunoglobulin isotypes in 4–6-wk-old *Lrrc8a*$^{-/-}$ mice and WT littermates determined by ELISA. (I) IgM and IgG3 serum antibody levels after immunization with TNP-LPS and TNP-Ficoll. Mice were immunized intraperitoneally with 10 µg TNP-LPS or 10 µg TNP-Ficoll on day 0 and bled on day 14. The level of antigen-specific antibody response in mice sera were analyzed by TNP-specific ELISA using 96-well plates coated with TNP-conjugated BSA at 10 µg/ml in PBS. Data are representative of three independent experiments with one mouse per group (A–C, E, and F), two independent experiments with three mice per group (D and G), six independent experiments with one mouse per group in five experiments and one *Lrrc8a*$^{-/-}$ mouse and two WT littermates in one experiment (H), and four independent experiments with one mouse per group in two experiments and two mice per group in two experiments (I). ELISAs were run on all samples simultaneously and were repeated twice. Each symbol represent mean OD value of an individual mouse in H. Mean and SEM are shown in B, D, and G–I. *, $P < 0.05$; **, $P < 0.01$; and ***, $P < 0.001$ (Student's *t* test). NS = not significant.

of the molecule are extracellular, rather than intracellular as has been suggested recently (Abascal and Zardoya, 2012). This conclusion was further supported by the observation that 293T cells transfected with a C-terminally FLAG-tagged LRRC8A demonstrated surface staining with anti-FLAG mAb (Fig. S1 B). FACS analysis using C18 antibody revealed that LRRC8A was expressed on the surface of mouse splenic CD3$^+$ T cells, B220$^+$ B cells, DX5$^+$ NK cells, CD14$^+$ macrophages, and CD11c$^+$ dendritic cells (Fig. 1 B and not depicted). FACS analysis of permeabilized splenic T and B cells revealed that a substantial amount of LRRC8A was intracellular (Fig. 1 B). Thymocytes and B cells in BM expressed surface LRRC8A at all stages of development, except for minimal, if any, expression on pro–B cells (Fig. 1, C and D). Thymocytes at all stages had the highest surface expression of LRRC8A of all immune cells studied. Similar results were obtained for all cell lineages using 4D10 mAb (unpublished data).

Generation and characterization of *Lrrc8a*$^{-/-}$ mice

The strategy for generating *Lrrc8a*$^{-/-}$ mice is depicted in Fig. S1 (C–F). LRRC8A was not detectable by immunoblotting thymocyte lysates from *Lrrc8a*$^{-/-}$ mice (Fig. S1 G) or by FACS analysis of splenic T and B cells from these mice (Fig. 1 E). *Lrrc8a*$^{-/-}$ mice were bred for 10 generations on the C57BL/6 background. Similar findings were obtained in *Lrrc8a*$^{-/-}$ mice generated from two independently targeted ES clones.

The frequency of live *Lrrc8a*$^{-/-}$ pups obtained from mating *Lrrc8a*$^{+/-}$ mice was 5.5% (Fig. 1 F). The frequency of *Lrrc8a*$^{-/-}$

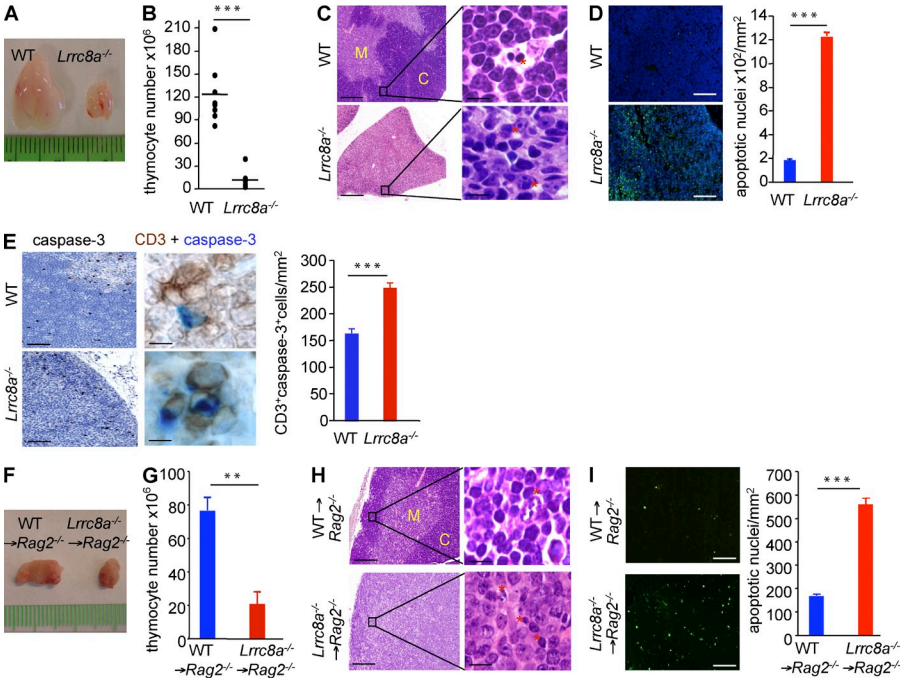

Figure 3. Decreased thymic cellularity and impaired thymocyte viability in *Lrrc8a*$^{-/-}$ mice. (A–E) Gross appearance (A), cellularity (B), H&E staining (C; bars: (left) 500 µm; (right) 30 µm; C = cortex, M = medulla; red asterisks in the inset indicate pyknotic nuclei), TUNEL staining (D, bars = 100 µm) with quantitative analysis of TUNEL$^+$ nuclei and immunostaining of thymic sections using a rabbit antibody that recognizes the p17 subunit, but not the precursor form, of caspase 3 (E, left; bars = 100 µm) or the rabbit anti-caspase 3 antibody combined with anti-CD3 (E, right; bars = 20 µm; caspase 3, blue and CD3, brown) with quantification of the results of thymi from *Lrrc8a*$^{-/-}$ mice and WT littermates (E). (F–I) Gross appearance (F), cellularity (G), H&E staining (H; bars: (left) 500 µm; (right) 30 µm; C = cortex, M = medulla; red asterisks in the inset indicate pyknotic nuclei), and TUNEL staining (I; bars = 100 µm) with quantitative analysis of TUNEL$^+$ nuclei of thymi from *Lrrc8a*$^{-/-}$→*Rag2*$^{-/-}$ (*Rag2*$^{-/-}$ mice reconstituted with *Lrrc8a*$^{-/-}$ BM) and WT→*Rag2*$^{-/-}$ (*Rag2*$^{-/-}$ mice reconstituted with WT BM) BM chimeras. Data are representative of eight experiments with one mouse per group (A and B), and three independent experiments with one mouse per group (C–I). Mean and SEM are shown in D–E, G, and I. **, $P < 0.01$; ***, $P < 0.001$.

embryos at E14.5 was ∼7.9% (n = 38), indicating increased early mortality in utero. *Lrrc8a*$^{-/-}$ mice had increased postnatal lethality; very few survived beyond 4 wk and none beyond 16 wk (Fig. 1 G). *Lrrc8a*$^{-/-}$ mice appeared normal at birth, but by the end of the first week of life, they showed persistent growth retardation (Fig. 1, H and I) although they fed normally. *Lrrc8a*$^{-/-}$ exhibited curly hair, hind limb weakness, progressive hydronephrosis, and sterility. Histological examination revealed epidermal hyperkeratosis, thin skeletal muscle bundles, vacuolated renal tubular cells, and absence of ovarian corpora lutea (Fig. 1 J). *Lrrc8a*$^{+/-}$ mice were comparable in appearance, size, and weight to WT littermates (Fig. 1, H and I) and had normal tissue histology (not depicted).

LRRC8A deficiency modestly impairs B cell development but not function

BM from *Lrrc8a*$^{-/-}$ mice had normal cellularity, modestly increased percentage of CD43$^+$B220^{low}IgM$^-$ pro–B cells, and modestly decreased percentages of CD43$^-$B220^{low}IgM$^-$ pre–B cells, CD43$^-$B220^{low}IgM$^+$ immature B cells, and B220^{hi}IgM^{hi} recirculating B cells (Fig. 2, A and B). *Lrrc8a*$^{-/-}$ mice had small spleens with well-preserved architecture (Fig. 2 C). The number of B220$^+$ cells in the spleen was approximately fourfold lower in *Lrrc8a*$^{-/-}$ mice compared with WT controls (Fig. 2 D). The percentage of splenic B220$^+$AnnexinV$^+$ cells was comparable in *Lrrc8a*$^{-/-}$ mice and WT controls (unpublished data). To exclude the potential contribution of extrinsic factors to the B cell lymphopenia in *Lrrc8a*$^{-/-}$ mice, we examined *Rag2*$^{-/-}$ chimeras reconstituted with either *Lrrc8a*$^{-/-}$ or WT BM cells. Splenic B cell numbers were similarly decreased in *Lrrc8a*$^{-/-}$→*Rag2*$^{-/-}$ chimeras compared with WT→*Rag2*$^{-/-}$ chimeras ($11.2 \pm 1.8 \times 10^6$ versus $47.9 \pm 3.6 \times 10^6$ cells, $n = 3$, $P < 0.01$), indicating that the peripheral B cell lymphopenia in *Lrrc8a*$^{-/-}$ mice is cell intrinsic.

FACS analysis of splenic B cell subsets (Carsetti et al., 2004) revealed comparable percentages of follicular B cells, but modestly decreased percentages of transitional B cells and marginal zone B cells in *Lrrc8a*$^{-/-}$ mice compared with WT littermates (Fig. 2 E). The numbers and subset distribution of peritoneal B220$^+$ B cells were normal in *Lrrc8a*$^{-/-}$ mice (Fig. 2 F).

Splenic B cells from *Lrrc8a*$^{-/-}$ mice proliferated normally to anti-IgM, anti-CD40, and LPS (Fig. 2 G). Except for a higher level of IgG2a, *Lrrc8a*$^{-/-}$ mice had normal levels of serum IgM, IgA, and IgG isotypes (Fig. 2 H) and mounted a normal antibody response to the type I T independent (TI) antigen TNP-LPS and the type II TI antigen TNP-Ficoll (Fig. 2 I). These results suggest that LRRC8A plays a minor role in B cell development and is important for peripheral B cell homeostasis but not B cell function.

LRRC8 deficiency results in decreased thymic cellularity and impaired thymocyte viability

The thymus was markedly smaller in *Lrrc8a*$^{-/-}$ mice compared with WT littermates (Fig. 3 A) and had an ∼10-fold reduction

in cellularity (Fig. 3 B). Examination of H&E-stained thymus sections demonstrated effacement of the corticomedullary junction and numerous pyknotic and karyorrhectic nuclei in *Lrrc8a*$^{-/-}$ mice (Fig. 3 C). TdT-mediated dUTP nick end labeling (TUNEL) demonstrated significantly increased numbers of apoptotic cells in *Lrrc8a*$^{-/-}$ thymi (Fig. 3 D). This was confirmed by the presence of increased numbers of CD3^{+} cells that co-stained for activated caspase 3 (Fig. 3 E). These results suggest that LRRC8A is important for thymocyte survival.

To exclude the effect of environmental factors on T cell development in *Lrrc8a*$^{-/-}$ mice, we examined thymi from *Rag2*$^{-/-}$ chimeras reconstituted with either *Lrrc8a*$^{-/-}$ or WT BM cells. Thymi of *Lrrc8a*$^{-/-}$→*Rag2*$^{-/-}$ chimeras were smaller and contained approximately fourfold fewer cells compared with thymi from WT→*Rag2*$^{-/-}$ control chimeras (Fig. 3, F and G). Histological analysis revealed impaired corticomedullary differentiation with increased numbers of karyorrhectic and apoptotic nuclei in thymi from *Lrrc8a*$^{-/-}$→*Rag2*$^{-/-}$ chimeras compared with thymi from control chimeras (Fig. 3, H and I).

Lrrc8a$^{-/-}$ mice have a cell-autonomous early block in thymocyte development

The distribution of double negative (DN), double positive (DP), and single positive (SP) subsets was comparable between *Lrrc8a*$^{-/-}$→*Rag2*$^{-/-}$ and control chimeras (Fig. 4 A). However, as expected from the reduced thymic cellularity, the numbers of CD4^{-}CD8^{-} DN, CD4^{+}CD8^{+} DP, and CD4^{+} and CD8^{+} SP thymocytes were reduced by approximately threefold in *Lrrc8a*$^{-/-}$→*Rag2*$^{-/-}$ chimeras compared with controls (Fig. 4 B). Analysis of DN subsets revealed a significant reduction in the numbers of CD44^{+}CD25^{+} DN2, CD44^{-}CD25^{+} DN3, and CD44^{-}CD25^{-} DN4 cells in *Lrrc8a*$^{-/-}$→*Rag2*$^{-/-}$ chimeras compared with controls (Fig. 4 C). The numbers of CD44^{+}CD25^{-} DN1 cells were decreased, but not significantly, in thymi from *Lrrc8a*$^{-/-}$→*Rag2*$^{-/-}$ chimeras. Irradiation can drive transiently the development of RAG2-deficient thymocytes in a restricted manner generating DP cells that express no surface CD3, but no SP cells, in the absence of donor-derived hematopoietic cells (Zúñiga-Pflücker et al., 1994). The DP and SP cells in the thymi of both chimeras were all CD3^{+} (unpublished data). Furthermore, irradiated *Rag2*$^{-/-}$ mice did not harbor DP or CD3^{+} thymocytes when examined at 8 wk (unpublished data). These results indicate that the defect in thymocyte development in *Lrrc8a*$^{-/-}$ mice is cell intrinsic.

The defect in the development of *Lrrc8a*$^{-/-}$ thymocytes could be due to increased cell death and/or decreased cell proliferation. The percentage of annexin V^{+} cells was significantly increased in *Lrrc8a*$^{-/-}$→*Rag2*$^{-/-}$ chimeras (Fig. 4 D), consistent with the increased number of apoptotic nuclei noted by TUNEL staining. In addition, BrdU incorporation in vivo was significantly decreased in thymocytes from *Lrrc8a*$^{-/-}$→*Rag2*$^{-/-}$ chimeras compared with controls (Fig. 4 E). Thymocyte proliferation to anti-CD3+IL-2 was significantly decreased *Lrrc8a*$^{-/-}$→*Rag2*$^{-/-}$ chimeras compared with control chimeras, but proliferation to PMA+ionomycin was comparable in the two groups (Fig. 4 F). Thus, LRRC8A expression by thymocytes is essential for their survival and proliferation.

Lrrc8a$^{-/-}$ mice exhibited a more exaggerated block in thymocyte development than *Lrrc8a*$^{-/-}$→*Rag2*$^{-/-}$ chimeras and a substantial decrease in the percentage of DP cells, reflected by a drastic decrease in their number compared with WT controls (Fig. 5, A and B). The decreased percentage of DP thymocytes and the resulting greater reduction in thymocyte numbers in *Lrrc8a*$^{-/-}$ mice compared with *Lrrc8a*$^{-/-}$→*Rag2*$^{-/-}$

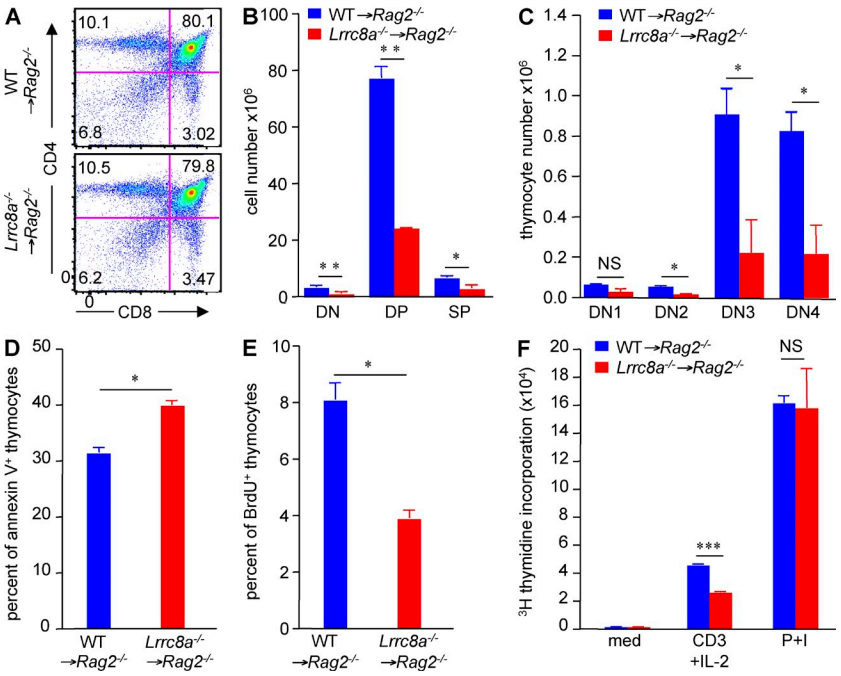

Figure 4. Cell-autonomous defect in thymocyte maturation in *Lrrc8a*$^{-/-}$ mice. (A–C) Representative FACS analysis of thymocytes with the percentage of cells found in each quadrant indicated (A), number of thymocyte subsets (B), and number of DN cell subsets (C) in the chimeras. (D and E) Percentage of annexin V^{+} cells (D) and of BrdU^{+} cells 3 h after i.p. injection of BrdU (E) in total thymocytes from the chimeras. (F) ^{3}H-thymidine incorporation in thymocytes from the chimeras in response to medium (med), anti-CD3+IL-2, and PMA+ionomycin (P+I) stimulation after 72 h in culture. Data are representative of three independent experiments with one mouse per group (A–F). Mean and SEM are shown in B–F. *, $P < 0.05$; **, $P < 0.01$; ***, $P < 0.001$ (Student's *t* test). NS = not significant.

chimeras suggest that extrinsic factors exacerbate the cell-intrinsic thymic phenotype in *Lrrc8a*$^{-/-}$ mice. DP thymocytes are exquisitely sensitive to damage by cytokines and hormones (Screpanti et al., 1989; Cohen, 1992; Ivanov and Nikolić-Zugić, 1998; Gruver and Sempowski, 2008). Serum chemistry profile and levels of TNF and cortisol levels were normal in *Lrrc8a*$^{-/-}$ mice (unpublished data). As in the *Lrrc8a*$^{-/-}$→*Rag2*$^{-/-}$ chimeras, the numbers of DN2-DN4, but not DN1, cells were significantly lower in *Lrrc8a*$^{-/-}$ mice than in WT controls (Fig. 5 C). The distribution of DN1a-e subsets, including the DN1a and DN1b early thymic progenitors (ETPs; Porritt et al., 2004), and the percentage of Lin$^-$Sca1$^+$c-kit$^+$ (LSK) cells in the BM which contain thymic multipotent progenitors (Ikuta and Weissman, 1992; Schwarz and Bhandoola, 2004) were comparable in *Lrrc8a*$^{-/-}$ and WT mice (Fig. 5, D and E). As in *Lrrc8a*$^{-/-}$→*Rag2*$^{-/-}$ chimeras, the percentage of annexin V$^+$ apoptotic thymocytes was increased and the BrdU incorporation in thymocytes was decreased significantly in *Lrrc8a*$^{-/-}$ mice compared with WT controls (Fig. 5, F and G). The percentage of TCR-γ/δ cells and the mean fluorescence intensity of the TCR-β chain on phenotypically mature thymocytes were comparable in *Lrrc8a*$^{-/-}$ mice and WT controls (Fig. 5, H and I). Unexpectedly, *Lrrc8a*$^{-/-}$ thymi had a significant increase in FOXP3$^+$ regulatory T (T reg) cells by immunohistochemistry staining and flow cytometry (Fig. 5, J and K).

LRRC8A deficiency impairs peripheral T cell expansion and function

Spleens of *Lrrc8a*$^{-/-}$→*Rag2*$^{-/-}$ chimeras were smaller (Fig. 6 A) and had an approximately fourfold decrease in the number of CD3$^+$ T cells compared with *WT*→*Rag2*$^{-/-}$ control chimeras (Fig. 6 B). The splenic CD4/CD8 ratio was comparable in *Lrrc8a*$^{-/-}$→*Rag2*$^{-/-}$ and control chimeras (Fig. 6 C). *Lrrc8a*$^{-/-}$→*Rag2*$^{-/-}$ chimeras had a significant decrease in the percentage of splenic CD4$^+$CD62L^{lo}CD44^{hi} T effector memory cells compared with control chimeras, and a compensatory increase in the percentage of CD4$^+$CD62L^{hi}CD44^{lo} naive T cells (Fig. 6 D). The proliferation of splenic T cells to immobilized anti-CD3 was significantly impaired in *Lrrc8a*$^{-/-}$→*Rag2*$^{-/-}$ chimeras compared with controls and was not increased by the addition of anti-CD28 mAb (Fig. 6 E). T cells from *Lrrc8a*$^{-/-}$→*Rag2*$^{-/-}$ chimeras proliferated normally in response to stimulation with PMA and ionomycin, indicating that they do not have a general intrinsic proliferative defect. These results indicate that LRRC8A is important for peripheral T cell expansion and function.

Like *Lrrc8a*$^{-/-}$→*Rag2*$^{-/-}$ chimeras, *Lrrc8a*$^{-/-}$ mice had a significant reduction in the number of splenic T cells compared with WT controls, with a normal CD4/CD8 ratio (Fig. 6, F and G). The percentage of splenic CD3$^+$Annexin V$^+$ cells was comparable in *Lrrc8a*$^{-/-}$ and WT mice (unpublished data).

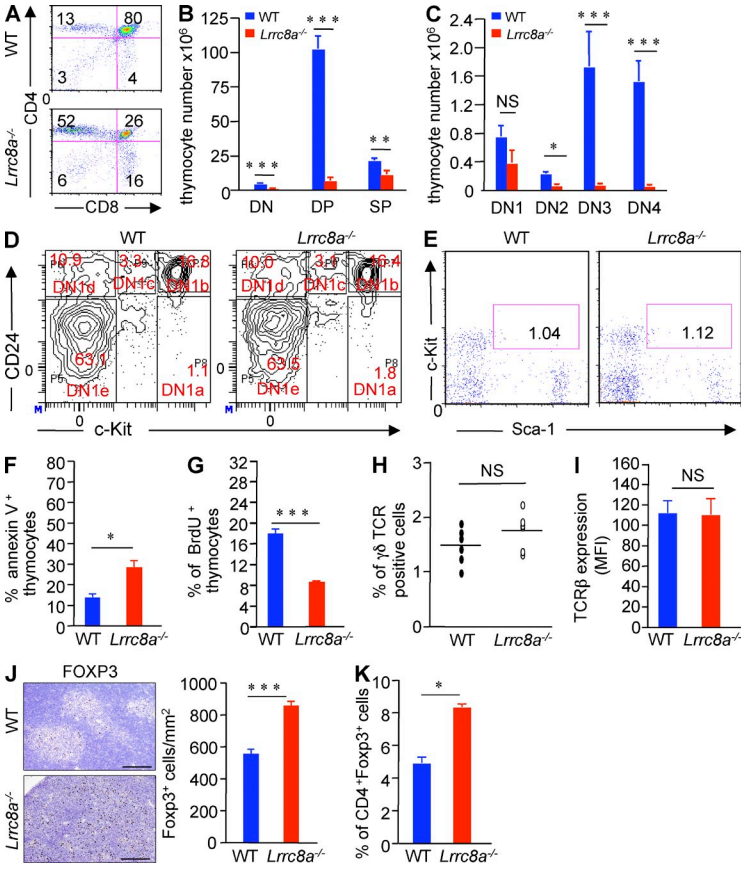

Figure 5. Defective thymocyte development in *Lrrc8a*$^{-/-}$ mice. (A) FACS analysis of CD4 and CD8 expression by thymocytes from a 3-wk-old *Lrrc8a*$^{-/-}$ mouse and WT littermate. The percentage of cells found in each quadrant is indicated. (B and C) Number of DN, DP, and SP thymocytes (B) and of Lineage-negative DN1, DN2, DN3, and DN4 thymocytes (C) in 3–6-wk-old *Lrrc8a*$^{-/-}$ mice and WT littermates. (D) FACS analysis of ETPs (DN1a-e) in the thymus. Lineage-negative DN1 thymocytes were resolved into ETP subpopulations by staining with c-kit and CD24. The percentage of cells found in each gate is indicated. (E) FACS analysis of Lin$^-$Sca1$^+$c-Kit$^+$ cells in the BM. (F and G) Percentage of annexin V$^+$ cells (F) and BrdU$^+$ cells 3 h after i.p. injection of BrdU (G) in thymocytes from 3–6-wk-old *Lrrc8a*$^{-/-}$ mice and WT littermates. (H) Percentage of TCR-γ/δ cells in the thymus of *Lrrc8a*$^{-/-}$ mice and WT controls. Each symbol represents an individual mouse and the small horizontal line indicates the mean. (I) Mean fluorescence intensity (MFI) of surface TCR-β chain expressed on phenotypically mature thymocytes. (J and K) Immunostain of FOXP3$^+$ cells (bars = 200 µm) and its quantitation (J) and percentage of FOXP3$^+$ cells in the CD4$^+$ cell population (K) in thymi from of *Lrrc8a*$^{-/-}$ mice and WT littermates. Data are representative of six independent experiments with one mouse per group (A, B, C, and H), and three independent experiments with one mouse per group (D–G and I–K). Mean and SEM are shown in B, C, F, G, and I–K. *, $P < 0.05$; **, $P < 0.01$; ***, $P < 0.001$ (Student's *t* test). NS = not significant.

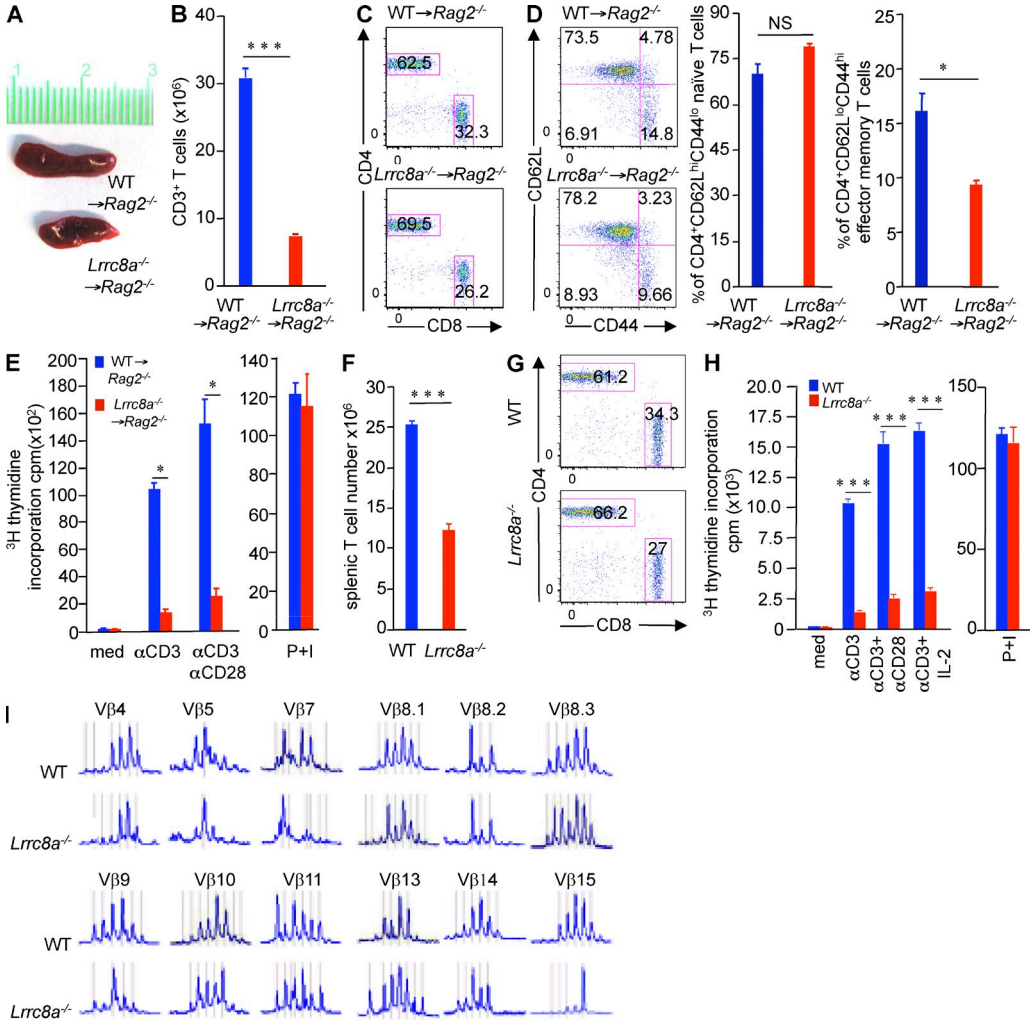

Figure 6. Cell-autonomous defect in peripheral T cell expansion and function in *Lrrc8a*$^{-/-}$ mice. (A–E) Gross appearance (scale = centimeter; A), T cell numbers (B), FACS analysis of CD4$^+$ and CD8$^+$ cells in gated CD3$^+$ T cells (C), FACS analysis of CD44 and CD62L expression by gated CD4$^+$ cells and percentages of CD4$^+$CD62^{hi}CD44^{lo} naive T cells and CD4$^+$CD62^{lo}CD44^{hi} T effector memory cells (D), and proliferation of T cells (E) from spleens of *Lrrc8a*$^{-/-}$→*Rag2*$^{-/-}$ and control WT→*Rag2*$^{-/-}$ chimeras. (F–H) Splenic T cell numbers (F), FACS analysis of CD4$^+$ and CD8$^+$ cells in gated splenic CD3$^+$ T cells (G), and proliferation of splenic T cells (H) from *Lrrc8a*$^{-/-}$ mice and WT control littermates. (I) Spectratyping analysis of CD3 diversity of selected TCR-Vβ families in splenic T cells from a 6-wk-old *Lrrc8a*$^{-/-}$ mouse and its WT littermate. med = medium. P + I = PMA+ionomycin. Data are representative of three independent experiments with one mouse per group (A–H), and two independent experiments with one mouse per group (I). Mean and SEM are shown in B, D–F, and H. *, $P < 0.05$; ***, $P < 0.001$ (Student's *t* test). NS = not significant.

However, splenic T cells from *Lrrc8a*$^{-/-}$ mice, like those from *Lrrc8a*$^{-/-}$→*Rag2*$^{-/-}$ chimeras, had significantly impaired proliferation to immobilized anti-CD3, which was not increased by the addition of anti-CD28 mAb or IL-2 (Fig. 6 H). Analysis of TCR-Vβ CDR3 diversity at 6 wk of age showed partial restriction of the T cell repertoire in *Lrrc8a*$^{-/-}$ mice compared with age-matched WT littermates, as indicated by skewed distribution for some (~25%), but not all, of the TCR-Vβ families analyzed (Fig. 6 I). The limited restriction of the TCR repertoire in *Lrrc8a*$^{-/-}$ mice is compatible with an abnormal TCR repertoire selection in the thymus and/or with abnormal clonal expansion/maintenance in the periphery.

LRRC8A is dispensable for the development and function of thymic epithelium

TECs play a critical role in thymic development (Rodewald, 2008). Because *Lrrc8a* is ubiquitously expressed, we examined TECs from *Lrrc8a*$^{-/-}$ mice. FACS analysis revealed that the percentages of CD45$^-$classII$^+$BP1$^+$ cortical TECs (cTECs) and CD45$^-$classII$^+$BP1$^-$ medullary TECs (mTECs) among CD45$^-$ nonlymphoid cells were comparable in *Lrrc8a*$^{-/-}$ mice and WT littermates (Fig. 7 A). Immunofluorescence staining confirmed the presence of both CK8$^+$CK5$^-$ cTECs and CK8$^-$CK5$^+$ mTECs in *Lrrc8a*$^{-/-}$ thymi (Fig. 7 B); however, their architectural distribution was abnormal with a very thin cortical layer and a disorganized medulla. In spite of the

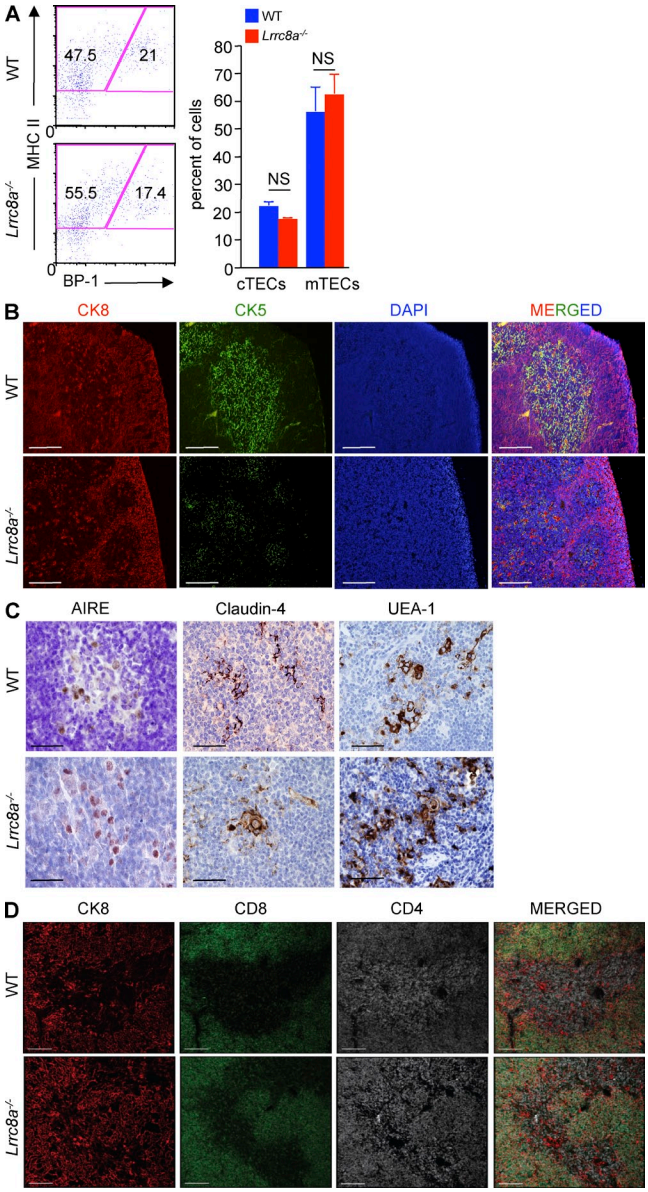

Figure 7. LRRC8A is dispensable for the development and function of thymic epithelium. (A) FACS analysis of MHC class II and BP-1 expression by CD45$^-$ cells. Numbers represent the percentage of cells. (B) Immunofluorescence staining of thymic sections (scale bars = 100 µm) for the cTEC antigen CK8, the mTEC antigen CK5, and the nuclear marker DAPI. (C) Expression of AIRE, claudin-4, and UEA-1 in thymi from *Lrrc8a*$^{-/-}$ and WT littermates (scale bars = 50 µm). (D) Immunofluorescence staining of WT and *Lrrc8a*$^{-/-}$ fetal thymi 8 wk after engraftment into the renal subcapsular space of WT recipient mice (bars = 100 µm). Data are representative of three independent experiments with one mouse per group (A–D). Mean and SEM are shown in A. NS = not significant.

architectural abnormalities, mTECs showed signs of maturation with expression of autoimmune regulator (AIRE), Claudin-4, and the ligand for ulex europeus agglutinin 1 (UEA-1; Fig. 7 C). Implantation of fetal thymic tissue from WT and *Lrrc8a*$^{-/-}$ mice into the kidney subcapsular region of 5-wk-old congenic mice supported comparable thymocyte development. Specifically, the grafts demonstrated corticomedullary differentiation with generation of SP T cell residents in the medulla (Fig. 7 D). Thus, LRRC8A is dispensable for the development of TECs and for their ability to support T cell development. However, a role for LRRC8A in dendritic cell–thymocyte interactions cannot be ruled out.

A ligand for LRRC8A is expressed by TECs and is important for the maturation of DN into DP thymocytes

We tested the hypothesis that a ligand for LRRC8A is expressed by TECs and is important for thymocyte maturation. Because of the kidney tubule abnormalities in *Lrrc8a*$^{-/-}$ mice, we initially examined whether the human embryonic kidney epithelial cell line 293T expresses an LRRC8A ligand. FACS analysis revealed increased binding of glutathione S-transferase (GST)–LRRC8A$_{343-810}$ fusion protein (GST-LRRC8A) to 293T cells, compared with GST (Fig. 8 A). This binding was specific because it was displaced by MBP-LRRC8A, but not by MBP (Fig. 8 A). Conversely, MBP-LRRC8A bound to 293T cells and was displaced by GST-LRRC8A but not GST (unpublished data). GST-LRRC8A did not bind to splenocytes (Fig. 8 B), further indicating the specificity of its binding to 293T cells. GST-LRRC8A bound to WT CD45$^-$ TECs, but not CD45$^+$ thymocytes, including DN, DP, and SP cells (Fig. 8, C and D). Both CD45$^-$classII$^+$BP1$^+$ cTECs and CD45$^-$classII$^+$BP1$^-$ mTECs bound GST-LRRC8A (Fig. 8 C). These results indicate that an LRRC8A ligand is expressed on nonhematopoietic cells, including TECs.

The BM-derived stromal cell line OP9 stably transfected with the Notch ligand Delta-like 1 (OP9-DL1) supports the differentiation and expansion of DN thymocytes into DP cells in the presence of IL-7 and Flt-3 ligand (Flt3L; Schmitt and Zúñiga-Pflücker, 2002). GST-LRRC8A specifically bound to OP9-DL1 (Fig. 8 E). Addition of GST-LRRC8A, but not GST alone, significantly inhibited the maturation of WT DN thymocytes into DP thymocytes in co-cultures with OP9-DL1 cells in the presence of IL-7 and Flt-3L (Fig. 8, F and G) and resulted in a higher percentage of annexin V$^+$ apoptotic DN and DP cells (Fig. 8 H). Inhibition of the DN to DP maturation by GST-LRRC8a was dose dependent (Fig. 8 I). These results suggest that interaction of LRRC8A in thymocytes with its ligand on OP9-DL1 cells is important for the in vitro maturation and survival of DN thymocytes into DP thymocytes.

LRRC8A associates with GRB2, GAB2, and LCK and activates AKT in thymocytes via the LCK–ZAP-70–GAB2–PI3K pathway

The kinase AKT has been implicated in the survival and proliferation of thymocytes (Chen et al., 2001; Juntilla et al., 2007). Given the increased cell death of LRRC8-deficient thymocytes, we examined whether LRRC8A activates AKT. Cross-linking of LRRC8A with anti-LRRC8A mAb resulted in AKT phosphorylation in WT thymocytes (Fig. 9 A), including DN thymocytes (Fig. 9 B). LRRC8A cross-linking failed to cause AKT phosphorylation in *Lrrc8a*$^{-/-}$ thymocytes (Fig. 9 C), but TCR/CD3 cross-linking caused normal AKT phosphorylation

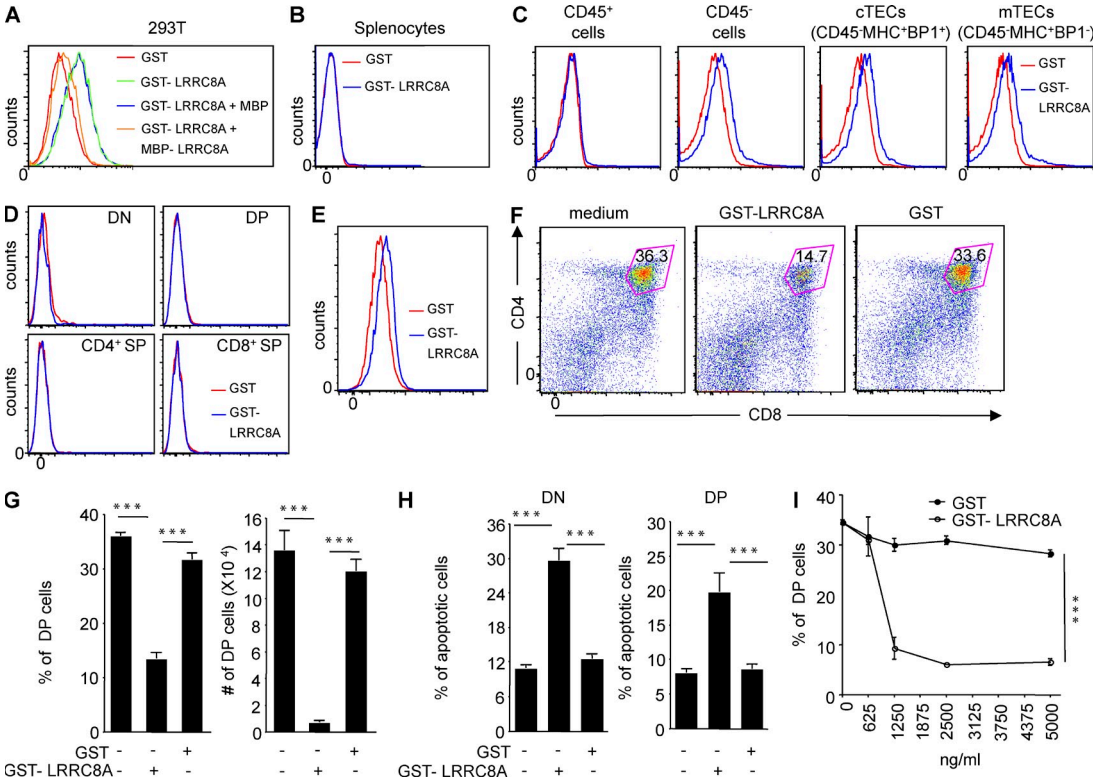

Figure 8. DN thymocyte maturation requires interaction of LRRC8A with a ligand expressed on TECs. (A–D) FACS analysis of the binding of GST-LRRC8A fusion protein to 293T cells (A), splenocytes (B), electronically gated CD45$^+$ and CD45$^-$ thymus cells, CD45$^-$MHCII$^+$BP-1$^+$ cTECs and CD45$^-$MHCII$^+$BP-1$^-$ mTECs from WT mice (C), DN, DP, and SP thymocytes from WT mice (D), and the OP9-DL1 stromal cell line (E). (F–H) FACS analysis of CD4 and CD8 expression by purified CD4$^-$CD8$^-$ DN thymocytes from WT mice after 4 d after co-culture with OP9-DL1 cells in the presence of medium, GST-LRRC8A, or GST as control (F), quantitation of the percentages and numbers of CD4$^+$CD8$^+$ DP cells recovered (G), and percentage of apoptotic cells in the DN and DP populations at the end of the 4 d co-culture as measured by Annexin V staining followed by flow cytometry (H). (I) Dose response curve of the effect of GST-LRRC8A on the in vitro differentiation of DN thymocytes co-cultured with OP9-DL1 cells. DN thymocytes were cultured on OP9-DL1 cells with GST or GST-LRRC8A at the indicated doses. The graph depicts frequency of DN cells after 4 d of culture. Data are representative of six independent experiments with one sample (A) and one mouse (B) per group, three independent experiments with one mouse per group (C and D), and one sample per group (E), and three independent experiments with three samples per group (F–I). Mean and SEM are shown in G–I. ***, $P < 0.001$ (Student's *t* test).

in these cells. LRRC8A-driven AKT phosphorylation in WT thymocytes was completely inhibited by LY294002 (Fig. 9 A), indicating that it was dependent on PI3 kinase (PI3K).

Both intracellular loops of LRRC8A lack the YXXM binding motif for binding PI3K. Receptors whose intracellular domain lacks this motif activate AKT by associating with the GRB2–GAB2 complex (Gu and Neel, 2003; Caron et al., 2009). GAB2 associates with the SRC kinases and is tyrosine phosphorylated by these kinases and ZAP-70 (Gu and Neel, 2003; Palacios and Weiss, 2007) on Y^{452}. This residue is part of the YXXM motif in GAB2 that recruits the p85 regulatory subunit of PI3K by interacting with its SH2 domain (Nishida et al., 1999; Zhao et al., 1999; Crouin et al., 2001). The first intracellular loop of LRRC8A contains a proline-rich region that could potentially interact with the SH3 domain of the adaptor GRB2 and SRC kinases. LRRC8A was found to be constitutively associated in thymocytes with GRB2, GAB2, and LCK (Fig. 9, D–F). Furthermore, LRRC8A ligation on thymocytes caused tyrosine phosphorylation of GAB2 at residue Y^{452}, LCK, and its substrate ZAP-70 (Fig. 9, G–I). The structurally different SRC kinase inhibitors PP2 and SU6656, and SYK/ZAP-70 inhibitors Piceatannol and R406, but not the MEK1/2 inhibitor GSK1120212, blocked LRRC8A-driven AKT phosphorylation in thymocytes (Fig. 9 J and not depicted). Furthermore, LRRC8A-driven AKT phosphorylation was diminished in *Zap70*$^{-/-}$ thymocytes (Fig. 9 K). These results indicate that LRRC8A constitutively associates with the GRB2–GAB2 complex and LCK, and activates AKT via the LCK–ZAP-70–GAB2–PI3K pathway.

We examined whether the lack of LRRC8A impairs AKT phosphorylation in thymocytes. Immunostaining sections of thymi fixed immediately after sacrifice revealed the presence of pAKT throughout the thymus in WT mice, with the subcapsular area giving the highest signal, but less intense pAKT staining in the thymus in *Lrrc8a*$^{-/-}$ mice (Fig. 10 A). pAKT staining was specific because it was abolished by preincubation with the specific phosphopeptide used for immunization (Fig. 10 B). Compared with WT thymi, *Lrrc8a*$^{-/-}$ thymi had a reduced percentage of pAKT-positive thymocytes, and a lower pAKT/AKT staining intensity ratio with a normal

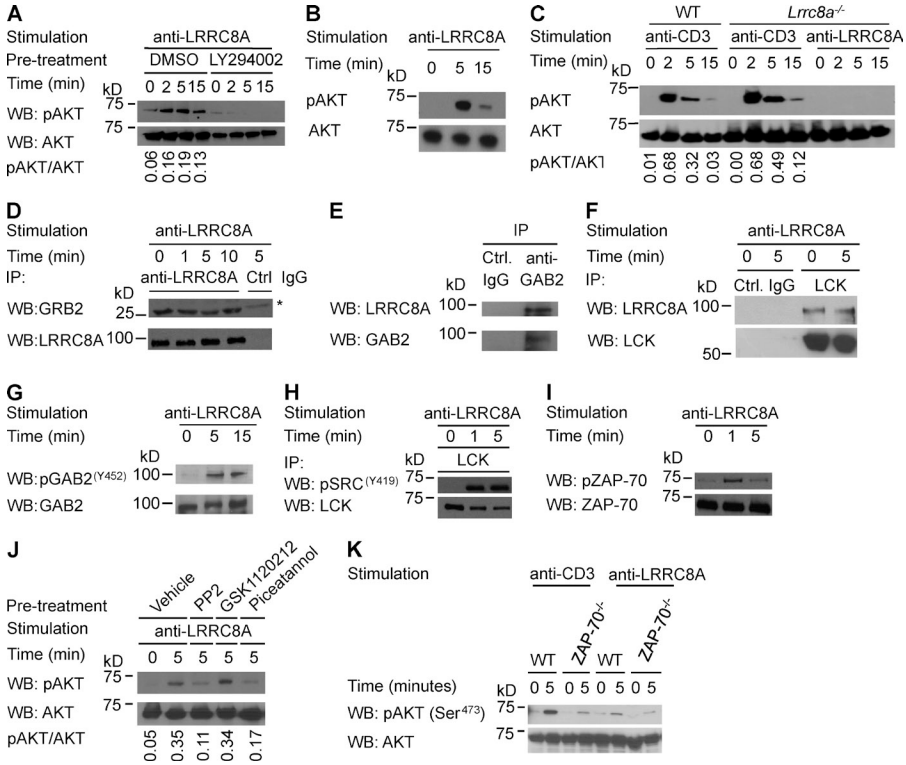

Figure 9. LRRC8A associates with GRB2, GAB2, and LCK, and activates AKT via the LCK–ZAP-70–GAB2–PI3K pathway in thymocytes. (A) AKT phosphorylation in WT thymocytes after LRRC8A ligation and the effect of the PI3 kinase inhibitor LY294002 on LRRC8A-mediated AKT phosphorylation. AKT phosphorylation in thymocytes pretreated with LY294002 or DMSO was determined by immunoblotting after LRRC8A ligation for the indicated times. (B) Immunoblot analysis of the phosphorylation of AKT in total DN thymocytes from WT mice after anti-LRRC8A stimulation. (C) AKT phosphorylation in thymocytes from *Lrrc8a*$^{-/-}$ mice in response to anti-LRRC8A and anti-CD3 cross-linking. CD3-stimulated WT thymocytes were used as controls. (D–F) Co-immunoprecipitation of LRRC8A with GRB2 (D), GAB2 (E), and LCK (F). Ctrl. = control. The asterisk in D indicates a nonspecific band in the control IgG lane. The total cell lysates were prepared from WT thymocytes. LRRC8A immunoprecipitates were immunoblotted for GRB2, and GAB2 and LCK immunoprecipitates were immunoblotted for LRRC8A. Isotype-matched irrelevant antibodies were used in immunoprecipitation as controls. (G–I) Phosphorylation of GAB2 (G), LCK (H), and ZAP-70 (I) after LRRC8A ligation on thymocytes. (J) AKT phosphorylation after LRRC8A ligation of thymocytes pretreated with the SRC kinase inhibitor PP2, the MEK1/2 inhibitor GSK1120212, and the SYK/ZAP-70 inhibitor Piceatannol. (K) LRRC8A- and TCR/CD3-driven AKT phosphorylation in thymocytes from WT or *Zap70*$^{-/-}$ mice after LRRC8A or TCR/CD3 ligation. Data are representative of three independent experiments with cells derived from one mouse per experiment (A, B, and D–J), and two independent experiments with cells derived from one mouse per group (C and K). The numbers below the blots in A, C, and J represent the mean ratio of pAKT/AKT in two (C) and three (A and J) experiments.

percentage of AKT-positive thymocytes (Fig. 10, C and D). The decreased AKT phosphorylation in *Lrrc8a*$^{-/-}$ thymi is specific because *Lrrc8a*$^{-/-}$ and WT thymi had comparable staining for pSTAT3 and STAT3 (Fig. 10, E and F). The percentage of thymocytes that stained with pAKT, but not of those that stained with AKT, was also markedly reduced in thymi from *Lrrc8a*$^{-/-}$→*Rag2*$^{-/-}$ chimeras compared with those from control chimeras (Fig. 10 G).

DISCUSSION

The present study demonstrates that LRRC8A plays a critical cell-autonomous role in T lymphocyte development and function. The thymus of *Lrrc8a*$^{-/-}$→*Rag2*$^{-/-}$ chimeras, like that of *Lrrc8a*$^{-/-}$ mice, had decreased cellularity, disorganized architecture, increased apoptosis, and decreased proliferation, indicating that these defects are T cell intrinsic. The decreased proliferation of thymocytes from *Lrrc8a*$^{-/-}$→*Rag2*$^{-/-}$ chimeras to anti–CD3+IL-2, but not to the TCR-independent stimuli PMA+ionomycin, suggests that LRRC8A signaling contributes to TCR-driven thymocyte proliferation. The numbers of thymocytes at the DN2 stage and beyond were significantly reduced in *Lrrc8a*$^{-/-}$→*Rag2*$^{-/-}$ chimeras, as in *Lrrc8a*$^{-/-}$ mice, indicating that the early block in thymocyte development is cell autonomous. Despite their defective T cell development and function, *Lrrc8a*$^{-/-}$→*Rag2*$^{-/-}$ chimeras had no increase in mortality, indicating that the runting and premature death of *Lrrc8a*$^{-/-}$ mice is likely due to their multiple organ abnormalities.

Our studies demonstrate that LRRC8A activates AKT via the LCK–ZAP-70–GAB2–PI3K pathway. LRRC8A constitutively associates with the GRB2–GAB2 complex and LCK. These associations may be direct, via interactions between the proline-rich region in the first intracellular domain of LRRC8A and the SH3 domain of GRB2 and LCK, and/or indirectly via the interaction of GAB2 with GRB2 and LCK (Gu and Neel, 2003). LRRC8A ligation caused phosphorylation of LCK and its substrate ZAP-70, and of their target GAB2 at residue Y^{452}, which, when phosphorylated, recruits PI3K to GAB2. The recruited PI3K undergoes phosphorylation by LCK and triggers AKT phosphorylation. LRRC8A-mediated activation of AKT was blocked by SRC, SYK/ZAP-70, and PI3K inhibitors. Thymocytes express both LCK and FYN. They also express both SYK and ZAP-70, with SYK expression highest in DN thymocytes and ZAP-70 expression highest in SP thymocytes (Chu et al., 1998; Palacios and Weiss, 2007). LRRC8A could use different SYK and SRC family kinase members to activate AKT.

AKT phosphorylation was markedly reduced in thymocytes from *Lrrc8a*$^{-/-}$ mice compared with thymocytes from WT controls. Given the established role of AKT in thymocyte survival, proliferation, and metabolism (Chen et al., 2001;

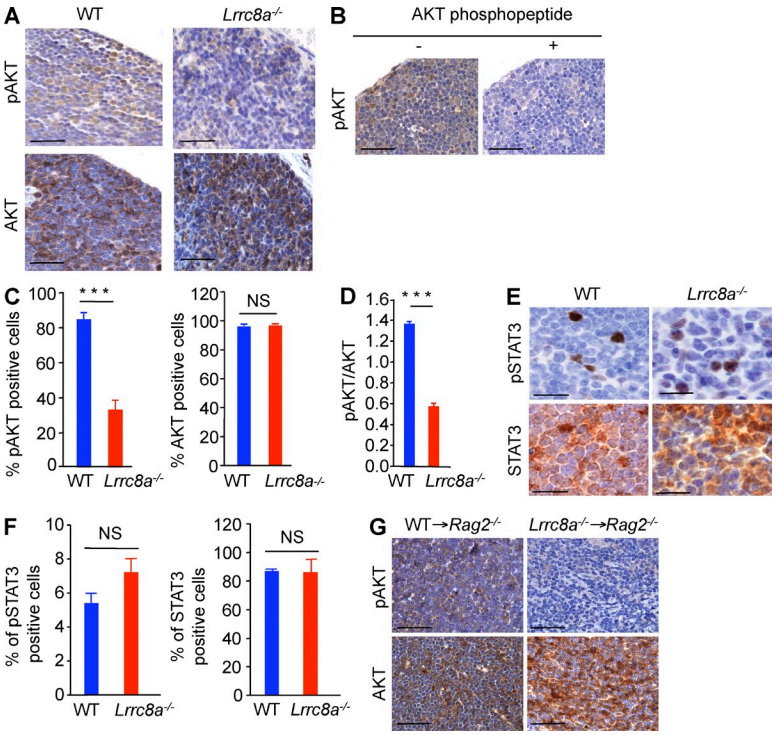

Figure 10. Lack of LRRC8A impairs AKT phosphorylation in thymocytes. (A–G) Immunostain for pAKT and AKT (A; bars = 30 µm), pAKT staining of WT thymus with anti-pAKT antibody in the absence or presence of the immunizing phosphopeptide (B; bars = 50 µm), percentage of pAKT-positive and AKT-positive cells (C), and pAKT/AKT staining intensity ratio (D) in thymic sections from 3-wk-old *Lrrc8a*$^{-/-}$ mice and WT littermates. (E and F) Staining for pSTAT3 and STAT3 (E; bars = 30 µm), and percentage of pSTAT3-positive and STAT3-positive cells (F) in thymic sections from 3-wk-old *Lrrc8a*$^{-/-}$ mice and WT littermates. (G) Immunostain for pAKT and AKT (bars = 50 µm). Thymic tissue sections derived from *Lrrc8a*$^{-/-}$→*Rag2*$^{-/-}$ and WT→*Rag2*$^{-/-}$ chimeras generated as in Fig. 3 were immunostained with pAKT and AKT specific antibodies. Data are representative of three independent experiments with one mouse per group (A, C, and D), and two independent experiments with one mouse per group (B and E–G). 200–300 cells in each group were counted in E. Mean and SEM are shown in C, D, and F. ***, $P < 0.001$ (Student's *t* test). NS = not significant.

Juntilla et al., 2007), the significant reduction in tonic AKT phosphorylation may play an important role in the defective thymic maturation of *Lrrc8a*$^{-/-}$ mice. Decreased AKT activation could also explain the relative increase in CD4^{+}FOXP3^{+} cells in thymus of these mice because AKT inhibits the generation of these cells (Haxhinasto et al., 2008; Merkenschlager and von Boehmer, 2010). The block in thymocyte maturation occurs earlier in *Lrrc8a*$^{-/-}$ mice than in *Akt1*$^{-/-}$/*Akt2*$^{-/-}$ mice, in which the DN3:DN4 transition is blocked (Juntilla et al., 2007). This could be explained by the fact that thymocytes from *Akt1*$^{-/-}$/*Akt2*$^{-/-}$ still express *Akt3* (Juntilla et al., 2007) and that LRRC8A ligation may deliver signals in addition to AKT that are important for thymocyte development and survival.

In addition to *Akt*, several genes have been implicated in early thymic development. They include *Notch 1* and its downstream targets *Hes1*, *Deltex*, *Nrap*, *and pTCR*α (Deftos et al., 1998, 2000; Krebs et al., 2001; Lamar et al., 2001), as well as *Bcl-2* (Deftos et al., 1998) and *Bcl11b* (Wakabayashi et al., 2003; Li et al., 2010). qPCR analysis revealed that the expression of these genes was either unaffected, or in a few cases increased, in DN1-DN4 thymocytes from *Lrrc8a*$^{-/-}$ mice compared with WT littermates (unpublished data). IL-7R signaling is important for the survival of early thymocytes (Peschon et al., 1994; Akashi et al., 1997; Kim et al., 1998). Surface expression of IL-7Rα by thymocyte subpopulations (DN1-4, DP, and SP) was comparable between *Lrrc8a*$^{-/-}$ mice and controls (unpublished data). These results rule out a role for abnormalities in the above pathways in the thymic developmental block caused by LRRC8A deficiency.

A ligand for LRRC8A was detected on TECs and on the stromal cell line OP9. A fusion protein containing GST and the extracellular domain of LRRC8A inhibited OP9-DL1 cell–dependent maturation of DN cells into DP cells in vitro. This finding, together with the decreased pAKT content of the thymus in *Lrrc8a*$^{-/-}$ mice, suggests that the putative LRRC8A ligand expressed by TECs delivers a critical survival signal via AKT to thymocytes. In addition to 293T cells, GST-LRRC8A bound to keratinocytes and fibroblasts (unpublished data), suggesting that disruption of LRRC8A interaction with a ligand expressed by epithelial and mesenchymal cells may contribute to the tissue pathology in *Lrrc8a*$^{-/-}$ mice. Identification of this ligand is currently the subject of investigation.

The reduced number of T cells and decreased percentage of CD4^{+} T effector memory cells in the spleen of *Lrrc8a*$^{-/-}$→*Rag2*$^{-/-}$ chimeras suggest that cell-intrinsic expression of LRRC8A in T cells is important for their homeostatic expansion in the periphery. The decreased proliferation of splenic T cells from these chimeras in response to TCR/CD3 ligation, but intact response to PMA+ionomycin, suggest that LRRC8A delivers a co-stimulatory signal to antigen-activated T cells. Indeed, ligation of LRRC8A causes AKT activation in normal splenic T cells (unpublished data), as it does in thymocytes. Lack of LRRC8A-driven AKT activation and/or maturation in an abnormal thymic environment may contribute to the decreased homeostatic proliferation and impaired function of LRRC8A-deficient peripheral T cells. Selective deletion of *Lrrc8a* in mature T cells is needed to distinguish between these two possibilities.

Lrrc8a$^{-/-}$ mice had a modest block in B cell development and normal B cell function. However, *Lrrc8a*$^{-/-}$ mice and *Lrrc8a*$^{-/-}$→*Rag2*$^{-/-}$ chimeras had a fourfold decrease in splenic B cells, suggesting that LRRC8A is important for peripheral B cell homeostasis. Ligation of LRRC8A caused AKT phosphorylation in B cells (unpublished data), and AKT is important for maintaining normal numbers of peripheral B cells (Juntilla et al., 2007). Thus, loss of LRRC8A-mediated AKT activation in B cells may have contributed to the peripheral B cell lymphopenia in *Lrrc8a*$^{-/-}$ mice.

In contrast to the *Lrrc8a*$^{-/-}$ mouse, the patient with the heterozygous *LRRC8A* mutation had no circulating B cells and agammaglobulinemia but normal numbers of circulating T cells (Sawada et al., 2003). The function of these T cells was not tested, but no opportunistic infections were reported in the patient despite an age of 17 yr. The difference in the two phenotypes most likely reflects the difference between the presence of a truncated mutant protein in the patient, which is thought to have acted as dominant negative (Conley, 2003; Sawada et al., 2003), and the complete absence of the protein in the knockout mouse. Given the 99% aa sequence homology between human and mouse LRRC8A, loss of *LRRC8A* expression in humans would likely present as severe combined immunodeficiency associated with multiple organ abnormalities.

MATERIALS AND METHODS

Generation of *Lrrc8a*$^{-/-}$ mice. We designed a gene-targeting construct for replacing the exon 3, which encodes the first 719 aa of LRRC8A. DNA fragments 4.809 and 3.375 kb in length were PCR amplified from a BAC clone DNA encoding the entire *Lrrc8a* gene (RP23-315H12) and cloned 5′ and 3′ in the pLNTK gene targeting vector. The linearized targeting construct was then electroporated into CJ7 ES cells, which were then selected in medium containing 0.4 mg/ml G418 and 10 mg/ml Gancyclovir. Of the three ES clones identified with targeted deletion of one of the two alleles of *Lrrc8a*, two were injected into C57BL/6 blastocysts for the generation of chimeric mice. ES cell clones and mice were genotyped by Southern blot and PCR. The LoxP-flanked *neo* selection cassette was then removed by breeding mice with EII Cre transgenic mice. All mice were kept in a pathogen-free environment. All procedures were performed in accordance with the Animal Care and Use Committee of the Boston Children's Hospital. All experiments used 4–6-wk-old *Lrrc8a*$^{-/-}$ mice and WT littermates. Due to the limited availability of *Lrrc8a*$^{-/-}$ mice and high pre- and postnatal mortality, many experiments were performed with one *Lrrc8a*$^{-/-}$ and one WT littermate and were repeated at least three times.

Anti-LRRC8A antibodies and immunoblotting. A polyclonal antibody (C18) was raised in rabbits against a C-terminal 18-aa-long peptide (NH_2-FSTLPPEVKERLWRADKE-COOH) sequence (aa 791–808) of LRRC8A and purified from using LRRC8A peptide Sepharose column chromatography. An LRRC8A-specific mouse mAb (4D10) was raised against the first extracellular loop (aa 147–262) of LRRC8A using standard protocols and purified from ascites by protein G column chromatography. Cell lysates were immunoblotted using C18 or 4D10 Abs, followed by HRP-conjugated goat anti–rabbit antibody or goat anti–mouse antibody conjugated to horseradish peroxidase–HRP and ECL.

Histology, immunohistochemistry, and immunofluorescence. Mouse tissue histopathology was performed at the Rodent Histopathology Core facility at the Harvard Medical School. TUNEL staining of thymic sections was performed as per the instructions of the manufacturer (BD). 2-µm-thick formalin-fixed paraffin-embedded sections were subjected to hematoxylin and eosin staining and immunohistological analysis. In brief, sections were dewaxed, rehydrated, and endogenous peroxidase activity blocked by 0.3% H_2O_2/methanol. Heat-induced antigen retrieval was performed when needed. Single immunostains were revealed by Real EnVision rabbit or mouse HRP Labeled Polymer system (Dako) or by preabsorbed biotinylated rabbit anti–rat mouse Ab (1:200; Vector), followed by Streptavidin (SA)-HRP conjugated and Diaminobenzidine (DAB; Dako), and nuclei were counterstained with hematoxylin. Bright field double immunostains were performed using Real EnVision Rabbit HRP (Dako) and MACH4 Universal AP Polymer kit (Biocare Medical) for the detection of CD3 and Caspase 3, respectively, and developed by either DAB or Ferangi Blue (DAKO). Nuclei were counterstained with methyl green. Double immunofluorescence analysis has been performed using secondary swine anti–rabbit FITC-conjugated antibody (1:30; Dako) for CK5 and rabbit anti–rat biotinylated antibody (1:200; Vector Laboratories), followed by Streptavidin–Texas red (1:100; Southern-Biotech) for CK8. Sections were then counterstained with DAPI. Digital images were acquired by a DP70 camera (Olympus) mounted on a Bx60 microscope (Olympus), using CellF Imaging software (Soft Imaging System GmbH). The following primary antibodies were used: rabbit anti-caspase 3 active (clone AF835, 1:600; R&D Systems), anti-CD3 (clone 2C11-145, 1:100; Dako), anti–cytokeratin-5 (clone D5/16 B4, 1:100; Covance), anti-AIRE (provided by P. Peterson, University of Tartu, Tartu, Estonia; 1:2,000), anti-pAKT (Ser 473; clone 736E11, 1:30; Cell Signaling Technology), anti-AKT (clone 11E7, 1:100; Cell Signaling Technology), anti-pSTAT3 (Tyr 705; clone D3A7, 1:80; Cell Signaling Technology), STAT3 (clone 79D7, 1:100; Cell Signaling Technology), rat anti–cytokeratin 8 (clone TROMA-I, 1:200; Developmental Studies Hybridoma Bank), anti-FOXP3 (clone F9, 1:100; Santa Cruz Biotechnology, Inc.), and mouse anti-CL4 (clone 3E2C1, 1:100; Invitrogen). In addition, biotinylated UEA-1 ligand (1:600; Vector Laboratories) was used to detect mature mTECs. The pAKT peptide used for immunization was used as a blocking peptide (Cell Signaling Technology) as a control for pAKT specificity.

Preparation of cells and flow cytometry. Single-cell suspensions from BM, thymus, and spleen of 3–6-wk-old mice were prepared as described earlier (de la Fuente et al., 2006). TECs were prepared as described by Gray et al. (2002).

Cells were stained with the appropriate fluorochrome-labeled mAbs and analyzed on a FACSCalibur or FACSCanto (BD). Fluorescent-labeled or biotinylated monoclonal antibodies to B220 (clone RA3-6B2), BP-1 (clone 6C3), CD3ε (clone 145-2C11), CD4 (clone L3T4), CD8 (clone 53–6.7), CD11b (clone M1/70), CD11c (clone N418), CD21/35 (clone eBio8D9), CD23 (clone B3B4), CD24 (clone M1/69), CD25 (clone 3C7), CD43 (clone eBioR260), CD44 (clone IM7), CD62L (clone MEL-14), CD71 (clone R17217), CD127 (clone A7R34), c-kit (clone 2B8), FOXP3 (clone FJK-16s), IgD (clone 11-26C), IgM (clone eB121-15F9), Sca-1 (clone D7), Ter-119 (clone Ter119), and Thy1.2 (clone 30-H12) were purchased from eBioscience. Anti–TCR-β (clone H57-597) was purchased from BD. Lineage-negative cells were identified by excluding cells stained with single fluorochrome-labeled cocktail of biotinylated B220 (clone RA3-6B2), CD3ε (clone 145-2C11), CD4 (clone L3T4), CD8 (clone 53–6.7), CD11b (clone M1/70), CD11c (clone N418), and Ter-119 (clone Ter119). Annexin-V staining kit from BioVision was used for the detection of apoptotic cells. Anti-FLAG mAb (clone M2) was purchased from Sigma-Aldrich. Intracellular staining was done as per the instructions provided with Cytoperm/Cytofix cell permeabilization and staining kit (BD).

BrdU incorporation assays. Mice were injected intraperitoneally with 1 mg BrdU in 100 µl 1× PBS and, 3 h later, tissues were harvested and BrdU incorporation was analyzed by using a BrdU Flow kit (BD).

Thymus transplantation and immunofluorescence. Individual thymus lobes from E14.5–18.5 WT and *Lrrc8a*$^{-/-}$ embryos were transplanted under the kidney capsule of anesthetized recipient mice. For staining cryosections, thymi were harvested, fixed in phosphate-buffered L-lysine with 1% paraformaldehyde/periodate (PLP), dehydrated in 30% sucrose in PBS, snap-frozen

in TBS tissue-freezing liquid (Triangle Biomedical Sciences), and stored at −80°C. Sections of 30-µm thickness were mounted on Superfrost Plus slides (Thermo Fisher Scientific) and stained with fluorescent mouse CD4 (GK1.5), mouse CD8α (53–6.7) antibodies (BD), and UEA-1 in a humidified chamber after Fc-receptor blockade with 1 µg/ml antibody 2.4G2 (Bio X Cell). Samples were mounted in FluorSave reagent solution (EMD Millipore) and stored at 4°C until analysis. Images were collected with a confocal microscopy system (Bio-Rad Laboratories) using a microscope (BX50WI; Olympus) and 10×/0.4 numerical aperture or 60×/1.2 numerical aperture water-immersion objective lenses. Images were analyzed with LaserSharp2000 software (Bio-Rad Laboratories), Volocity (Perkin Elmer), and Imaris (Bitplane).

Proliferation and activation of thymocytes and splenic T and B cells. Thymocytes were prepared as described earlier (de la Fuente et al., 2006). Splenic T and B cells were purified by negative selection using kits from Miltenyi Biotec. Thymocytes and purified T cells were cultured in medium alone or in wells coated with 2 µg/ml anti-CD3 monoclonal antibody (clone KT3; Abcam) with or without 2 µg/ml anti-CD28 (clone L293; BD) or 40 ng/ml IL-2 (PeproTech). PMA (Sigma-Aldrich) was used at 50 ng/ml, and ionomycin (Sigma-Aldrich) was used at 0.5 µM. Purified B cells were cultured in medium alone or in the presence of goat $F(ab')_2$ anti–mouse IgM (Jackson ImmunoResearch Laboratories, Inc.), 2 µg/ml anti-CD40 (R&D Systems), or 10 µg/ml LPS (Sigma-Aldrich). 72 h later, the cells were pulsed with 1 µCi [^{3}H]thymidine and counted.

TCR-Vβ repertoire analysis. TCR-Vβ repertoire clonality determination on splenic T cells was performed using spectratyping by BioMed Immunotech, Inc.

Generation of LRRC8A fusion proteins and analysis of binding of LRRC8A fusion protein to cells. LRRC8A C-terminal polypeptide (aa 343–810) was fused downstream of GST and MBP (maltose binding protein) in pGEX-4T1 (GE Healthcare) and pMAL-c2G (New England Biolabs, Inc.) expression vectors, respectively. Fusion proteins were expressed in recommended bacterial hosts. Expressed GST-LRRC8A and MBP-LRRC8A fusion proteins were purified as per the manufacturer's instructions. Target cells were incubated with GST/GST-LRRC8A or MBP/MBP-LRRC8A on ice for 30 min. The binding of LRRC8A fusion proteins was detected using flow cytometry by staining cells with the appropriate fluorochrome-labeled anti-tag antibody (anti-GST antibody [clone 26H1; Cell Signaling Technology] or anti-MBP antibody [clone MBP-17; Sigma-Aldrich]).

In vitro maturation of DN to DP thymocytes. Purified DN thymocytes were cultured on monolayers of OP9-DL1 cells (gift from J.C. Zúñiga-Pflücker, University of Toronto, Toronto, Canada) in recombinant IL-7 and Flt3L (PeproTech) containing medium in the presence of either GST/GST-LRRC8A or MBP/MBP-LRRC8A for 4–6 d as described earlier (Schmitt and Zúñiga-Pflücker, 2002), after which cells were harvested and analyzed by FACS.

LRRC8A signaling studies. For cell stimulation, purified cells were incubated with the respective antibodies on ice for 20 min and cross-linked with $F(ab')_2$ fragments of appropriate secondary antibodies for indicated time points at 37°C. Immediately after stimulation, the cells were lysed in SDS sample buffer by adding one-fourth volume of 5× SDS lysis buffer directly into the cell suspensions. Samples were boiled for 5 min and separated by 4–15% SDS-PAGE and evaluated by immunoblotting using anti-pAKT (clone DE9, 1:1,000; Cell Signaling Technology), anti-AKT (clone 11E7, 1:1,000; Cell Signaling Technology), anti-pGAB2 (Y^{452}, clone C33G1, 1:1,000; Cell Signaling Technology), anti-GAB2 (clone 26B6, 1:1,000; Cell Signaling Technology), anti-pSRC (Y^{416}, clone D49G4, 1:1,000; Cell Signaling Technology), anti-LCK (clone L22B1, 1:1,000; Cell Signaling Technology), anti–pZAP-70 (Y^{493}, 1:1,000; Cell Signaling Technology), anti–ZAP-70 (clone D1C10E, 1:1,000; Cell Signaling Technology), or anti-GRB2 (clone c-23; Santa Cruz Biotechnology, Inc.) antibody. PP2 and Su6656 (SRC inhibitors) were purchased from EMD Millipore. Piceatannol and R406 (SYK inhibitors) were purchased from Selleckchem Chemicals, LLC. Wortmannin and Ly294002 (PI3K inhibitors) were purchased from Sigma-Aldrich. GSK1120212 (MEK1/2 inhibitor) was purchased from BioVision Technology, Inc. LRRC8A and LCK immunoprecipitations were performed as described earlier (de la Fuente et al., 2006) using anti-LRRC8A antibodies and anti-LCK mouse monoclonal antibody (clone 3A5; Santa Cruz Biotechnology, Inc.), respectively. Cell activation marker expression, thymocytes, and splenic B and T cell proliferation and cytokine production assays were performed as described previously (de la Fuente et al., 2006).

Serum immunoglobulins and antibody measurements. Serum immunoglobulins and antibody levels were determined by previously described methods. Mice were immunized with KLH prepared with Imject Alum (Thermo Fisher Scientific), TNP-Ficoll, or TNP-LPS (Bio-Rad Laboratories). ELISA assays were performed to estimate specific immunoglobulins levels in the serum samples of the immunized mice as earlier (de la Fuente et al., 2006).

Quantitative RT-PCR. Total RNA was prepared from the flow cytometrically–sorted WT and KO DN1-4 thymocytes using the RNAqueous extraction kit (Ambion). RT-PCR was performed using the iScript cDNA synthesis kit (Bio-Rad Laboratories). Carboxyfluorescein (FAM)-labeled specific TaqMan primers were purchased from Applied Biosystems. Quantitative PCR reactions were run on an ABI Prism 7300 sequence detection system platform (Applied Biosystems). The housekeeping gene β_2-microglobulin was used as a control. The relative gene expression among the different samples was determined using the method described by Pfaffl (2001). Quantities of all targets in test samples were normalized to the corresponding β_2-microglobulin levels.

Statistical analysis. Statistical analysis of the data using the Student's *t* test or analysis of variance (ANOVA) was performed with Prism software (GraphPad Software Inc.).

Online supplemental material. Fig. S1 shows surface expression of LRRC8A in untransfected and LRRC8A-transfected 293T cells by FACS using LRRC8A and FLAG tag–specific antibodies and the strategy to generate *Lrrc8a*$^{-/-}$ mice. Online supplemental material is available at http://www.jem.org/cgi/content/full/jem.20131379/DC1.

We thank Drs. Stuart H. Orkin, Yuko Fujiwara, and Mayumi Kaku (Center for Molecular Hematology at Children's Hospital supported by NIDDK DK49216) for help in generating the *LRRC8a*$^{-/-}$ mice, Dr. Rodrick T. Bronson (Harvard Medical School) for his help in mouse necropsy analysis, Dr. Vijaya Ramesh (Massachusetts General Hospital, Boston) for help in generating mAb 4D10, Drs. Luigi D. Notarangelo, T. Chatila, N. Ramesh, and Michel Massaad for helpful discussions, and Ms. Tatyana Sannikova and Elena Fontana for providing expert technical assistance.

This work was supported by USPHS grants AI-183503 (R.S. Geha), AI-79769, and Eleanor and Miles Shore 50th Anniversary Career Development Award (L. Kumar); K12 HD052896, Talecris Fellowship Award and AAAAI Fellow Career Development Award (J. Chou); T32 AI-007512 (J. Chou and C.S.K. Yee); a grant from Fondazione Cariplo (P.L. Poliani); and AI-069259 and AI-078897 (U.H. von Andrian).

The authors declare no competing financial interests.

Submitted: 1 July 2013
Accepted: 21 March 2014

REFERENCES

Abascal, F., and R. Zardoya. 2012. LRRC8 proteins share a common ancestor with pannexins, and may form hexameric channels involved in cell-cell communication. *Bioessays*. 34:551–560. http://dx.doi.org/10.1002/bies.201100173

Akashi, K., M. Kondo, U. von Freeden-Jeffry, R. Murray, and I.L. Weissman. 1997. Bcl-2 rescues T lymphopoiesis in interleukin-7 receptor-deficient mice. *Cell*. 89:1033–1041. http://dx.doi.org/10.1016/S0092-8674(00)80291-3

Caron, C., K. Spring, M. Laramée, C. Chabot, M. Cloutier, H. Gu, and I. Royal. 2009. Non-redundant roles of the Gab1 and Gab2 scaffolding adapters in VEGF-mediated signalling, migration, and survival of endothelial cells. *Cell. Signal.* 21:943–953. http://dx.doi.org/10.1016/j.cellsig.2009.02.004

Carsetti, R., M.M. Rosado, and H. Wardmann. 2004. Peripheral development of B cells in mouse and man. *Immunol. Rev.* 197:179–191. http://dx.doi.org/10.1111/j.0105-2896.2004.0109.x

Chen, W.S., P.Z. Xu, K. Gottlob, M.L. Chen, K. Sokol, T. Shiyanova, I. Roninson, W. Weng, R. Suzuki, K. Tobe, et al. 2001. Growth retardation and increased apoptosis in mice with homozygous disruption of the Akt1 gene. *Genes Dev.* 15:2203–2208. http://dx.doi.org/10.1101/gad.913901

Chu, D.H., C.T. Morita, and A. Weiss. 1998. The Syk family of protein tyrosine kinases in T-cell activation and development. *Immunol. Rev.* 165:167–180. http://dx.doi.org/10.1111/j.1600-065X.1998.tb01238.x

Cohen, J.J. 1992. Glucocorticoid-induced apoptosis in the thymus. *Semin. Immunol.* 4:363–369.

Conley, M.E. 2003. Genes required for B cell development. *J. Clin. Invest.* 112:1636–1638. http://dx.doi.org/10.1172/JCI20408

Cressman, D.E., K.C. Chin, D.J. Taxman, and J.P. Ting. 1999. A defect in the nuclear translocation of CIITA causes a form of type II bare lymphocyte syndrome. *Immunity.* 10:163–171. http://dx.doi.org/10.1016/S1074-7613(00)80017-5

Crouin, C., M. Arnaud, F. Gesbert, J. Camonis, and J. Bertoglio. 2001. A yeast two-hybrid study of human p97/Gab2 interactions with its SH2 domain-containing binding partners. *FEBS Lett.* 495:148–153. http://dx.doi.org/10.1016/S0014-5793(01)02373-0

de la Fuente, M.A., L. Kumar, B. Lu, and R.S. Geha. 2006. 3BP2 deficiency impairs the response of B cells, but not T cells, to antigen receptor ligation. *Mol. Cell. Biol.* 26:5214–5225. http://dx.doi.org/10.1128/MCB.00087-06

Deftos, M.L., Y.W. He, E.W. Ojala, and M.J. Bevan. 1998. Correlating notch signaling with thymocyte maturation. *Immunity.* 9:777–786. http://dx.doi.org/10.1016/S1074-7613(00)80643-3

Deftos, M.L., E. Huang, E.W. Ojala, K.A. Forbush, and M.J. Bevan. 2000. Notch1 signaling promotes the maturation of CD4 and CD8 SP thymocytes. *Immunity.* 13:73–84. http://dx.doi.org/10.1016/S1074-7613(00)00009-1

Gray, D.H., A.P. Chidgey, and R.L. Boyd. 2002. Analysis of thymic stromal cell populations using flow cytometry. *J. Immunol. Methods.* 260:15–28. http://dx.doi.org/10.1016/S0022-1759(01)00493-8

Gruver, A.L., and G.D. Sempowski. 2008. Cytokines, leptin, and stress-induced thymic atrophy. *J. Leukoc. Biol.* 84:915–923. http://dx.doi.org/10.1189/jlb.0108025

Gu, H., and B.G. Neel. 2003. The "Gab" in signal transduction. *Trends Cell Biol.* 13:122–130. http://dx.doi.org/10.1016/S0962-8924(03)00002-3

Haxhinasto, S., D. Mathis, and C. Benoist. 2008. The AKT-mTOR axis regulates de novo differentiation of $CD4^+Foxp3^+$ cells. *J. Exp. Med.* 205:565–574. http://dx.doi.org/10.1084/jem.20071477

Ikuta, K., and I.L. Weissman. 1992. Evidence that hematopoietic stem cells express mouse c-kit but do not depend on steel factor for their generation. *Proc. Natl. Acad. Sci. USA.* 89:1502–1506. http://dx.doi.org/10.1073/pnas.89.4.1502

Inohara, C., C. Chamaillard, McDonald, and G. Nuñez. 2005. NOD-LRR proteins: role in host-microbial interactions and inflammatory disease. *Annu. Rev. Biochem.* 74:355–383. http://dx.doi.org/10.1146/annurev.biochem.74.082803.133347

Ivanov, V.N., and J. Nikolić-Zugić. 1998. Biochemical and kinetic characterization of the glucocorticoid-induced apoptosis of immature $CD4^+CD8^+$ thymocytes. *Int. Immunol.* 10:1807–1817. http://dx.doi.org/10.1093/intimm/10.12.1807

Juntilla, M.M., J.A. Wofford, M.J. Birnbaum, J.C. Rathmell, and G.A. Koretzky. 2007. Akt1 and Akt2 are required for αβ thymocyte survival and differentiation. *Proc. Natl. Acad. Sci. USA.* 104:12105–12110. http://dx.doi.org/10.1073/pnas.0705285104

Kim, K., C.K. Lee, T.J. Sayers, K. Muegge, and S.K. Durum. 1998. The trophic action of IL-7 on pro-T cells: inhibition of apoptosis of pro-T1, -T2, and -T3 cells correlates with Bcl-2 and Bax levels and is independent of Fas and p53 pathways. *J. Immunol.* 160:5735–5741.

Kobe, B., and A.V. Kajava. 2001. The leucine-rich repeat as a protein recognition motif. *Curr. Opin. Struct. Biol.* 11:725–732. http://dx.doi.org/10.1016/S0959-440X(01)00266-4

Krebs, L.T., M.L. Deftos, M.J. Bevan, and T. Gridley. 2001. The Nrarp gene encodes an ankyrin-repeat protein that is transcriptionally regulated by the notch signaling pathway. *Dev. Biol.* 238:110–119. http://dx.doi.org/10.1006/dbio.2001.0408

Lamar, E., G. Deblandre, D. Wettstein, V. Gawantka, N. Pollet, C. Niehrs, and C. Kintner. 2001. Nrarp is a novel intracellular component of the Notch signaling pathway. *Genes Dev.* 15:1885–1899. http://dx.doi.org/10.1101/gad.908101

Lee, M.S., and Y.J. Kim. 2007. Signaling pathways downstream of pattern-recognition receptors and their cross talk. *Annu. Rev. Biochem.* 76:447–480. http://dx.doi.org/10.1146/annurev.biochem.76.060605.122847

Li, L., M. Leid, and E.V. Rothenberg. 2010. An early T cell lineage commitment checkpoint dependent on the transcription factor Bcl11b. *Science.* 329:89–93. http://dx.doi.org/10.1126/science.1188989

Merkenschlager, M., and H. von Boehmer. 2010. PI3 kinase signalling blocks Foxp3 expression by sequestering Foxo factors. *J. Exp. Med.* 207:1347–1350. http://dx.doi.org/10.1084/jem.20101156

Nishida, K., Y. Yoshida, M. Itoh, T. Fukada, T. Ohtani, T. Shirogane, T. Atsumi, M. Takahashi-Tezuka, K. Ishihara, M. Hibi, and T. Hirano. 1999. Gab-family adapter proteins act downstream of cytokine and growth factor receptors and T- and B-cell antigen receptors. *Blood.* 93:1809–1816.

Palacios, E.H., and A. Weiss. 2007. Distinct roles for Syk and ZAP-70 during early thymocyte development. *J. Exp. Med.* 204:1703–1715. http://dx.doi.org/10.1084/jem.20070405

Peschon, J.J., P.J. Morrissey, K.H. Grabstein, F.J. Ramsdell, E. Maraskovsky, B.C. Gliniak, L.S. Park, S.F. Ziegler, D.E. Williams, C.B. Ware, et al. 1994. Early lymphocyte expansion is severely impaired in interleukin 7 receptor-deficient mice. *J. Exp. Med.* 180:1955–1960. http://dx.doi.org/10.1084/jem.180.5.1955

Pfaffl, M.W. 2001. A new mathematical model for relative quantification in real-time RT-PCR. *Nucleic Acids Res.* 29:e45. http://dx.doi.org/10.1093/nar/29.9.e45

Porritt, H.E., L.L. Rumfelt, S. Tabrizifard, T.M. Schmitt, J.C. Zúñiga-Pflücker, and H.T. Petrie. 2004. Heterogeneity among DN1 prothymocytes reveals multiple progenitors with different capacities to generate T cell and non-T cell lineages. *Immunity.* 20:735–745. http://dx.doi.org/10.1016/j.immuni.2004.05.004

Rodewald, H.R. 2008. Thymus organogenesis. *Annu. Rev. Immunol.* 26:355–388. http://dx.doi.org/10.1146/annurev.immunol.26.021607.090408

Sawada, A., Y. Takihara, J.Y. Kim, Y. Matsuda-Hashii, S. Tokimasa, H. Fujisaki, K. Kubota, H. Endo, T. Onodera, H. Ohta, et al. 2003. A congenital mutation of the novel gene LRRC8 causes agammaglobulinemia in humans. *J. Clin. Invest.* 112:1707–1713. http://dx.doi.org/10.1172/JCI18937

Schmitt, T.M., and J.C. Zúñiga-Pflücker. 2002. Induction of T cell development from hematopoietic progenitor cells by delta-like-1 in vitro. *Immunity.* 17:749–756. http://dx.doi.org/10.1016/S1074-7613(02)00474-0

Schwarz, B.A., and A. Bhandoola. 2004. Circulating hematopoietic progenitors with T lineage potential. *Nat. Immunol.* 5:953–960. http://dx.doi.org/10.1038/ni1101

Screpanti, I., S. Morrone, D. Meco, A. Santoni, A. Gulino, R. Paolini, A. Crisanti, B.J. Mathieson, and L. Frati. 1989. Steroid sensitivity of thymocyte subpopulations during intrathymic differentiation. Effects of 17 β-estradiol and dexamethasone on subsets expressing T cell antigen receptor or IL-2 receptor. *J. Immunol.* 142:3378–3383.

Smits, G., and A.V. Kajava. 2004. LRRC8 extracellular domain is composed of 17 leucine-rich repeats. *Mol. Immunol.* 41:561–562. http://dx.doi.org/10.1016/j.molimm.2004.04.001

Tang, J., S. Stern-Nezer, P.C. Liu, L. Matyakhina, M. Riordan, N.L. Luban, P.J. Steinbach, and S.G. Kaler. 2004. Mutation in the leucine-rich repeat C-flanking region of platelet glycoprotein Ibβ impairs assembly of von Willebrand factor receptor. *Thromb. Haemost.* 92:75–88.

Wakabayashi, Y., H. Watanabe, J. Inoue, N. Takeda, J. Sakata, Y. Mishima, J. Hitomi, T. Yamamoto, M. Utsuyama, O. Niwa, et al. 2003. Bcl11b is required for differentiation and survival of alphabeta T lymphocytes. *Nat. Immunol.* 4:533–539. http://dx.doi.org/10.1038/ni927

Zhao, C., D.H. Yu, R. Shen, and G.S. Feng. 1999. Gab2, a new pleckstrin homology domain-containing adapter protein, acts to uncouple signaling from ERK kinase to Elk-1. *J. Biol. Chem.* 274:19649–19654. http://dx.doi.org/10.1074/jbc.274.28.19649

Zúñiga-Pflücker, J.C., D. Jiang, P.L. Schwartzberg, and M.J. Lenardo. 1994. Sublethal γ-radiation induces differentiation of $CD4^-/CD8^-$ into $CD4^+/CD8^+$ thymocytes without T cell receptor β rearrangement in recombinase activation gene 2-/- mice. *J. Exp. Med.* 180:1517–1521. http://dx.doi.org/10.1084/jem.180.4.1517